

Implementation of a hybrid Lagrangian Filtered Density Function-Large Eddy Simulation methodology in a dynamic adaptive mesh refinement environment

Laura Pereira de Castro,¹ Abigail Paula Pinheiro,¹ Vitor Vilela,¹ Gabriel Marcos Magalhães,¹ Ricardo Serfaty,² and João Marcelo Vedovotto^{1, a)}

¹⁾*School of Mechanical Engineering, Federal University of Uberlândia;
Av. João Naves de Ávila, 2121, Uberlândia, MG, Brazil,
38400-902*

²⁾*Petrobras SA, Rio de Janeiro, RJ, Brazil, 21941-915*

(Dated: 29 March 2021)

Multi-species mixing processes play an important role in many engineering, biological, and environmental applications. Since simulating mixing flows can be useful to understand its physics and to study industrial issues, this work aims to develop the basis of a methodology able to simulate the physics of multiple-species mixing flows, using a hybrid Large Eddy Simulation (LES) / Lagrangian Filtered Density Function (FDF) method on an adaptive, block-structured mesh. A computational model of notional particles transport on a distributed processing environment is built using a parallel Lagrangian map. This map connects the Lagrangian information with the Eulerian framework of the in-house code MFSim, in which transport equations are solved. The Lagrangian composition FDF method, through the Monte Carlo technique, performs algebraic calculations over an ensemble of notional particles and provides composition fields statistically equivalent to those obtained by Finite Volume numerical solution of partial differential equations (PDE). Finally, to maintain high accuracy in the system of Stochastic Differential Equations SDE solver when an Adaptive Mesh Refinement (AMR) environment is used, a methodology for ensuring mass conservation is developed to preserve at least the statistical moments up to order two, even in the case of annihilation or cloning of a large number of notional particles in one time step, ensuring the applicability of Lagrangian FDF methods in dynamically adaptive grid refinement.

^{a)}Electronic mail: vedovotto@ufu.br

I. INTRODUCTION

Multi-species mixing flows can be noticed everywhere: in a cup of tea, individual species mix with water until becoming a homogeneous fluid; in a car exhaust system and an industry chimney, the hot combustion products outflow to atmosphere and mix with pure air; and in many industrial processes, different fluids mix each other to create a specific product.

To simulate this kind of flows, a hybrid Large Eddy Simulation (LES) / Lagrangian composition Filtered Density Function (FDF) method on adaptive, block-structured mesh (AMR) is presented in this work. The LES [1] approach solves the large scales of the flow, while the small ones are modeled. The Lagrangian FDF method [2], on the other hand, provides the chemical species composition fields using the Monte Carlo method [3], in which a system of stochastic equations is solved. Moreover, the AMR is used to numerically solve the filtered transport equations and to represent the FDF composition by notional particles. Using adaptive mesh ensures the requirements of LES and Monte Carlo methods to achieve acceptable results i.e., to increase accuracy in regions of flow with more turbulent intensity and with sharp variations in composition field, respectively.

The AMR methods can be useful in different kinds of problems, e.g. [4–11]. For solving fluid-dynamics problems, this technique is not new [12 and 13], and, since its early development, it showed a great potential to capture detailed phenomenon. Furthermore, using adaptive mesh can greatly contribute to minimize the required computational resources and the simulation time because it distributes cell nodes heterogeneously throughout the flow domain, reducing the total number of cells necessary to represent the whole computational domain. AMR methods locally refine the mesh in regions in which the error in the solution is above some threshold previously specified. These methods can be applied either to structured or unstructured meshes. An example of unstructured adaptive mesh refinement for solving the NavierStokes equations is the Moving Mesh Interface Tracking (MMIT) Method of [14], and more recently, the work of [15] demonstrate the applicability of AMR to a multiphysics framework using the Finite Element Method on unstructured grids. Regarding structured grids, the most fundamental approach for mesh adaptation is to use a non-uniform structured grid, which consists in using different grid spacing along the domain. This approach is usually applied to multiblock or chimera grids [16].

AMR strategies may also be employed with Cartesian grids, usually via octree [17 and 18]

or Structured Adaptive Mesh Refinement (SAMR) [12 and 19]. Both methods are based on splitting Cartesian cells in order to obtain a locally refined mesh at some regions of interest. However, in the SAMR approach, cells located at a given refinement level are clustered into Cartesian blocks, or patches. These patches are organized in a hierarchy of Cartesian grids with different levels of refinement which cover the entire domain, concentrating the finer grids at regions which require special attention. A level of refinement comprises one or more Cartesian grid blocks which do not intersect each other and share the same grid spacing. Since the refined regions are grouped as Cartesian blocks, the method can take advantage of uniform mesh solvers, which may be applied individually to each block. The structured feature of SAMR is particularly important for the coupling of the Lagrangian and the Eulerian approaches since it facilitates the particle tracking procedures such as filtered properties interpolation to the notional particles and recovery of statistical moments from the particles to the Eulerian grid. In the present work, the strategy of the SAMR approach adopted is based on the classical work of [12, 19, and 20].

Despite the numerous applications of AMR to fluid-dynamics problems, to the best knowledge of the authors, the literature lacks information about how to preserve statistical data when a particle-based methodology is used in an adaptive mesh environment. The present paper is focused on non-reactive mixing flows. However, the described mathematical and numerical models are not restricted to those simplifications. The methodology here presented can be used to solve a wide range of flows, such as reactive ones. The hybrid LES/FDF method has a great advantage when applied to reactive flows, since it models in a closed way the chemical reaction term of species transport equations [3, 21, and 22].

To that extent, in this paper, the authors aim to expose the development of a parallel Lagrangian composition FDF code and its merging with the in-house code MFSim ([16, 23–25]. The FDF code performs algebraic calculations over an ensemble of notional particles using the Monte Carlo method and produces composition fields statistically equivalent to those obtained by Finite Volume numerical solution of partial differential equations (PDE) [21, 26, and 27]. The complete Computational Fluid Dynamics (CFD) code allowed us to implement the aforementioned hybrid method and to simulate mixing flows.

The first step towards achieving this main objective is building a computational model of notional particles on a distributed processing environment by means of a parallel Lagrangian map, which can hold different types of Lagrangian elements, including notional particles [22].

The map connects the Lagrangian information with the Eulerian framework of the MFSim code, in which transport equations are solved. The developed Lagrangian framework uses a multi-level hash table based on *Uthash* [28] that is built according to the Eulerian mesh. Uthash is a C header file which provides tools to create and manipulate hash tables and it is useful to quickly manage data. In the present work, it is proposed a method to conserve at least the statistical moments up to the second order two, even in the case of annihilation or cloning of a large number of particles in one time step.

The paper is organized as follows. In Section II, the FDF methodology is presented as well as a brief overview of the mathematical modeling employed. The Lagrangian Map and its coupling in the MFSim data structure is described in details in Section III, as well as the parallelization procedure for the Lagrangian framework. Section IV exposes the developed Lagrangian composition FDF code, which communicates with the Finite Volume framework of the MFSim code. The Lagrangian Monte Carlo algorithm that is applied upon the system of stochastic differential equations to solve the composition field of the flow ia described and the central point of MC solver, namely the population of notional particles constraint, is covered. Finally, the results obtained using the methodology proposed in the present work are showed in Section V. First, the Partially Stirred Reactor concept and a single box PaSR simulation are presented. Then, the statistical equivalence between Eulerian and Lagrangian approaches is evaluated.

II. MATHEMATICAL MODELING

A. Set of filtered equations

The following simplifying assumptions are considered to derive the mathematical model: (a) fluid is considered as Newtonian, (b) body forces, heat transport by radiation, Soret and Dufour effects are not addressed, and (c) heat losses are neglected. In addition, the mathematical model considers multi-species variable-density reactive flows, in which the primary transported variables are the Reynolds filtered density $\bar{\rho}$, the mass-weighted Favre filtered three velocity components \tilde{u}_i , specific enthalpy \tilde{h} and mass fractions \tilde{Y}_k of the k chemical species ($k = 1, \dots, K$), where K is the number of species. Under the previously

mentioned conditions, the balance equations are:

$$\frac{\partial \bar{\rho}}{\partial t} + \frac{\partial \bar{\rho} \tilde{u}_j}{\partial x_j} = 0, \quad (1)$$

$$\frac{\partial \bar{\rho} \tilde{u}_i}{\partial t} + \frac{\partial \bar{\rho} \tilde{u}_j \tilde{u}_i}{\partial x_j} = \frac{\partial \bar{T}_{ij}}{\partial x_j} - \frac{\partial \tau_{ij}^{SGS}}{\partial x_j}, \quad (2)$$

$$\frac{\partial \bar{\rho} \tilde{\phi}_\alpha}{\partial t} + \frac{\partial \bar{\rho} \tilde{u}_j \tilde{\phi}_\alpha}{\partial x_j} = \frac{\partial \bar{Q}_{\alpha,j}}{\partial x_j} - \frac{\partial Q_{\alpha,j}^{SGS}}{\partial x_j} + \bar{S}_\alpha, \quad (3)$$

where the variable ϕ_α denotes the mass fraction of a chemical species or the enthalpy of the mixture, $(x_i, i = 1, 2, 3)$ are the spatial coordinate, and t is the time. $\bar{T}_{ij} = \bar{\tau}_{ij} - \bar{p} \delta_{ij}$ is the tensor of mechanical constraints including both a deviatoric (shear stresses τ_{ij}) and a spheric (pressure $\bar{p} \delta_{ij}$) contribution, while $\bar{Q}_{\alpha,j}$ denotes the component of the molecular diffusion flux of the scalar α in the direction j . In the above expression, $\tau_{ij}^{SGS} = (\bar{\rho} u_i \bar{u}_j - \bar{\rho} \tilde{u}_i \tilde{u}_j)$ is the subgrid scale (SGS) stress tensor and $Q_{\alpha,j}^{SGS} = (\bar{\rho} u_i \bar{\phi}_\alpha - \bar{\rho} \tilde{u}_i \tilde{\phi}_\alpha)$ represents the SGS scalar flux components, respectively. Finally, the last term in the RHS of Eq. (3), i.e. \bar{S}_α , denotes the filtered reaction rate. The above system is closed by an additional equation of state: $P = P_0(t) + \bar{p}(\mathbf{x}, t)$, with $P_0(t)$ the thermodynamic pressure.

The unresolved momentum fluxes are expressed according to the Boussinesq assumption, $\tau_{ij}^{SGS} - \delta_{ij} \tau_{kk}^{SGS}/3 = 2\mu_{SGS} (\tilde{S}_{ij} - \delta_{ij} \tilde{S}_{kk}/3)$, where μ_{SGS} is the subgrid scale viscosity, and $\tilde{S}_{ij} = (\partial \tilde{u}_i / \partial x_j + \partial \tilde{u}_j / \partial x_i)/2$ is the strain rate tensor of the resolved field [29 and 30]. The eddy viscosity μ_{SGS} is obtained from the Dynamic Smagorinsky closure [31]. The SGS scalar flux is represented with a gradient law, $\bar{Q}_{\alpha,j} = -\bar{\rho} \Gamma_{SGS} \partial \tilde{\phi}_\alpha / \partial x_j$, where $\tilde{\phi}_\alpha$ is the resolved scalar field and Γ_{SGS} denotes the subgrid diffusion coefficient evaluated from $\Gamma_{SGS} = \bar{\rho} (C_s \Delta)^2 |\tilde{S}| / Sc_{SGS}$ with Sc_{SGS} a subgrid scale turbulent Schmidt number.

The accurate determination of the filtered chemical reaction rate \bar{S}_α remains one of the most important challenges when applying LES to turbulent reactive flows. It is used herein a formulation that accounts for the subgrid-scale fluctuations of the chemical composition through a modeled transport equation for the subgrid-scale FDF, which provides an effective resolution to the closure problems that arise from averaging or filtering the highly nonlinear chemical source terms [22]. Since one-point and one-time FDF models are used, the terms that involve two points information, for instance some property gradients, are not explicitly resolved. Hence, important effects, such as molecular diffusion and viscous effects, and associated dissipation phenomena require to be modeled.

B. FDF methodology

The joint velocity-composition FDF transport equations are an alternative mathematical model for the physical system usually treated in an Eulerian reference frame. This model considers both the momentum and composition fields in a probabilistic manner. The joint FDF transport equation may be written as [32]:

$$\frac{\partial f_{\Delta, u_i \Phi}}{\partial t} + \frac{\partial u_j f_{\Delta, u_i \Phi}}{\partial x_j} = -\frac{\partial}{\partial v_j} [\langle A_i | v_i, \Psi \rangle_{\Delta} f_{\Delta, u_i \Phi}] - \frac{\partial}{\partial \psi_{\alpha}} [\langle \Theta_{\alpha} | v_i, \Psi \rangle_{\Delta} f_{\Delta, u_i \Phi}]. \quad (4)$$

The joint FDF is valuable because it can be used to derive all one-point statistics of the random velocity vector u_i and the random species mass fraction array Φ belonging to a range in the sample spaces v_i and Ψ , e.g., the filtered velocity \hat{u}_i , the filtered composition $\hat{\phi}_{\alpha}$, the Reynolds stresses $\hat{u}_i \hat{u}_j$, the composition fluxes $\hat{u}_i \Phi'_{\alpha}$ and the filtered chemical reaction rate \hat{S}_{α} .

Since the joint velocity-composition FDF transport equation has random variables describing three velocity components u_i and the array of chemical species Φ , when Eq. (4) is integrated over the velocity sample space v_i , it results in the composition FDF transport equation Eq. (5).

$$\begin{aligned} \frac{\partial f_{\Delta, \Phi}}{\partial t} + \frac{\partial \langle u_j \rangle_{\Delta} f_{\Delta, \Phi}}{\partial x_j} &= -\frac{\partial [\langle u_j \Psi \rangle_{\Delta} - \langle u_j \rangle_{\Delta}] f_{\Delta, \Phi}}{\partial x_j} \\ &\quad + \frac{\partial}{\partial \psi_{\alpha}} \left[\left\langle \frac{\partial}{\partial x_j} \left(\Gamma \frac{\partial \Phi}{\partial x_j} \right) \middle| \Psi \right\rangle_{\Delta} f_{\Delta, \Phi} \right] - \frac{\partial [S_{\alpha}(\Phi) f_{\Delta, \Phi}]}{\partial \psi_{\alpha}}, \end{aligned} \quad (5)$$

whose unclosed terms must be modeled. These terms are the SGS advective flux and the diffusion term, in which this expresses the influence of molecular diffusion on FDF transport. These terms are the first and second terms of the right-hand-side of Eq. (5), respectively. The last right hand side term is a closed form of the chemical reaction rate. The final form of the composition FDF transport equation, with all closures applied, is:

$$\begin{aligned} \frac{\partial f_{\Delta, \Phi}}{\partial t} + \frac{\partial \langle u_j \rangle_{\Delta} f_{\Delta, \Phi}}{\partial x_j} &= \frac{\partial}{\partial x_j} \left((\Gamma + \Gamma^{SGS}) \frac{\partial f_{\Delta, \Phi}}{\partial x_j} \right) \\ &\quad + \frac{\partial}{\partial \psi_{\alpha}} [\Omega_m (\psi_{\alpha} - \langle \Phi_{\alpha} \rangle_{\Delta}) f_{\Delta, \Phi}] - \frac{\partial [S_{\alpha}(\Phi) f_{\Delta, \Phi}]}{\partial \psi_{\alpha}}, \end{aligned} \quad (6)$$

where $\Omega_m = C_{\omega}(\Gamma + \Gamma_{sgs})/\Delta^2$ is the turbulent frequency determined by LES, C_{ω} is a mechanical-to-scalar time-scale ratio, which is assumed to be constant. The standard value, 2.0, is based on the local equilibrium assumption between production and dissipation of variance in isotropic turbulence for constant-density flows [33]. However, C_{ω} may assume higher

values depending on thermal expansion effects, resulting in density variations in turbulent flames [22].

C. Stochastic Differential Equations

In the Lagrangian FDF approach, the flow properties are represented by an ensemble of notional particles [3]. It is possible to consider each stochastic notional particle as a realization of the turbulent reactive flow, which is a discrete representation of the Eulerian PDF (Eq. 6). Each of these particles transports its own ensemble of independent variables, e.g., position in the physical space and composition of the scalar field. Each particle is also subjected to a system of stochastic differential equations (SDE). Given a sample of particles, the results obtained from the statistical moments are obtained by construction of the SDEs equivalent to those that would be obtained with the solution of the Eulerian PDF. A general framework for the construction of SDEs that are equivalent to the PDF transport equation is given in [34].

The following system of stochastic differential equations models the general diffusion process [26]:

$$dX_i(t) = D_i(\vec{X}(t), t) dt + E(\vec{X}(t), t) dW_i(t), \quad (7)$$

where $E \equiv \sqrt{2(\Gamma + \Gamma^{SGS})}$, and $D_i \equiv \langle u_i \rangle_\Delta + \partial(\Gamma + \Gamma^{SGS})/\partial x_i$, and $dW(t)$ is a statistical independent increment, e.g., the Wiener noise. One can see that the filtered velocity and the SGS molecular diffusivity are required from the Eulerian field.

The stochastic equation that describes the evolution of particles composition is:

$$\frac{d\phi_\alpha^*}{dt} = -\Omega_m(\phi_\alpha^* - \langle \phi_\alpha \rangle_\Delta) + S_\alpha, \quad (8)$$

where ϕ_α^* is the α species composition of the notional particle. The term that comprises this frequency is the Interaction by Exchange with the Mean (IEM) micromixing model [3]. Eqs. (7) and (8) are numerically treated separately due to simplicity and to preserve the Markovian character of the diffusion process [27]:

$$X_i^p(t_{n+1}) = X_i^p(t_n) + D_i^p(t_n) \Delta t + E^p(t_n) \Delta t^{1/2} \xi_i^p(t_n), \quad (9)$$

where n stands for the current time step, p represents the particle and ξ_i^p is a random variable with normalized Gaussian distribution.

D. Coupling of the hybrid model solvers

As previously mentioned, one main advantage of the PDF-based transported methods is the accuracy in evaluating the chemical reactions rates, since it is presented closed in its transport equation. Although the simulation of reactive flows is out scope of the present paper, the same methodology here presented can be used to simulate reactive flows, which are a further step in the authors' research line.

Along with the simplifying hypothesis presented in section II A, the following assumptions are also made in order to obtain a non-dimensional reaction rate of a single, global and irreversible chemical reaction:

1. Combustion of a single, global ($m = 1$) irreversible ($k_m^r = 0$) reaction, i.e., $C + rO \rightarrow (1 + r)P$, where C represents the fuel, O the oxidizer, premixed, P the combustion products and r the mass of oxidizer necessary to react a unity of mass of fuel,
2. The fuel C is the minor species reactant, i.e., $[X_C] \ll [X_O]$. As a consequence, the oxidant mass fraction is $Y_O = \dot{m}_O / \dot{m}_O + \dot{m}_C \approx 1 = cte$,
3. The molecular diffusivity of the fuel and the thermal diffusivity of the mixture are equivalents, i.e. unitary Lewis number, $Le = \lambda / \rho c_p \Gamma = 1$,
4. Low Mach number flow, $Ma \ll 1$,
5. The exponent of temperature of the Arrhenius law is null ($\beta_1 = 0$)

In the context of premixed flames, the chemical reaction progress variable is defined as:

$$c = \frac{T - T_u}{T_b - T_u}, \quad (10)$$

where T is the temperature, T_u is the temperature of unburnt (fresh) gases and T_b is the temperature of the burnt gases. A value of $c = 0$ is associated to fresh gases, and $c = 1$ corresponds to burnt gases.

Under the assumptions used in this section, once given the parameters $\tau = (T_b - T_u)/T_b$ and $\beta = \tau(T_a/T_b)$, where $T_a = E_a/R$ is the activation temperature, E_a is the activation energy and R is the universal constant of gases, the structure of a stationary premixed flame depends on the "flame parameter" Λ :

$$\Lambda = \frac{\alpha A_\tau T_u^{\beta_1}}{S_L^2} \exp^{-\frac{\beta}{\tau}}. \quad (11)$$

Such a parameter contains information like heat diffusivity, $\alpha = \lambda/(\rho C_p)$, rate parameters, A_τ , laminar flame speed S_L .

Under those hypothesis, the chemical reaction rate, $S(c)$, is related to the rate of progress of the single, global reaction, q , and the non-dimensional chemical rate of production, $\dot{\mathcal{S}}$, by the expression $S(c) = A_\tau \rho \dot{\mathcal{S}}$, where the pre-exponential constant can be calculated as $A_\tau = \Lambda S_L^2 / [\alpha e^{(-\beta/\tau)}]$ and $\dot{\mathcal{S}} = (1 - c) \exp[-(\beta(1 - c))/(1 - \tau(1 - c))]$. It is noteworthy that the term $S(c)$ presents a strongly non-linear dependency on β , τ and of the progress variable c .

It is important to note that due the simplifying hypothesis retained in the present work concerning the transport equations and chemical kinetics, the effects of the chemical reaction on the flow are exclusively noted by the density variations generated by the thermal expansion. In the Eulerian field, it is possible to solve a transport equation for the filtered progress variable \tilde{c} :

$$\frac{\partial \bar{\rho} \tilde{c}}{\partial t} + \frac{\partial \bar{\rho} \tilde{u}_j \tilde{c}}{\partial x_j} = \frac{\partial}{\partial x_j} \left(\bar{\rho} (\Gamma + \Gamma_{SGS}) \frac{\partial \tilde{c}}{\partial x_j} \right) + \bar{S}(c), \quad (12)$$

where the filtered chemical reaction rate term $\bar{S}(c)$ is evaluated in the Lagrangian framework when the flow is reactive.

One advantage of adopting a Lagrangian approach is that the central statistical moments of the progress variable, c , can be readily recovered by the Monte Carlo simulation retained for the solution of the system generated by Eqs. (7) and (8). It is worth noting that the filtered progress variable, \tilde{c} , can be evaluated from the first central moment of c . In the case of the second central moment, i.e., the variance of the filtered progress variable, the modeled transport equation, $\widetilde{c''^2}$, is given by:

$$\begin{aligned} \frac{\partial \bar{\rho} \widetilde{c''^2}}{\partial t} + \frac{\partial \bar{\rho} \tilde{u}_i \widetilde{c''^2}}{\partial x_i} &= \frac{\partial}{\partial x_i} \left[\bar{\rho} (\Gamma + \Gamma_{SGS}) \frac{\partial \widetilde{c''^2}}{\partial x_i} \right] + 2\bar{\rho} (\Gamma + \Gamma_{SGS}) \frac{\partial \tilde{c}}{\partial x_i} \frac{\partial \tilde{c}}{\partial x_i} \\ &\quad - 2C_\Omega \Omega_m \widetilde{c''^2} + 2\overline{(c - \tilde{c})} \bar{S}(c). \end{aligned} \quad (13)$$

The turbulent transport, production, dissipation and reaction terms in the equation for the variance of the progress variable c , Eq. (13), are modeled in the same way as in the LES framework. It noteworthy also that the molecular diffusion terms becomes negligible once

the flows of interest are classified as having characteristic high Reynolds number. Moreover, as it will be seen in the results section, the mesh adopted for the simulations performed has a sufficiently large local Reynolds number. In other words, the mesh size adopted has at least ten times the size of the Kolmogorov length scale.

The importance of Eqs. (12) and (13) is based on the fact that the Eulerian and Lagrangian approaches must be equivalent. This is a matter of validation of the Lagrangian approach and it will be further discussed. In the absence of chemical reactions, the terms dependent on $\bar{S}(c)$ become zero, and, hence, the comparison between the solutions of the SDEs and the Eulerian approach serves as a validation procedure for the implementations. It is important to point out that in respect to the verification and validation of the MFSim's Eulerian solver, the interested reader may be refer to [16, 23–25, 35–37].

III. LAGRANGIAN MAP

A. Eulerian / Lagrangian link

The computational model of a system, preceded by the physical, mathematical and numerical models, is crucial considering the quality of a Computational Fluid Dynamics (CFD) software. The Eulerian / Lagrangian modeling requires a data structure able to exchange information between these two frameworks. Moreover, the direct access to the ensemble of particles contained in each cell is essential to the Lagrangian FDF code performance, especially regarding algorithms dependent on sorting [3].

Two questions arise when the transport of particles in Eulerian domain is taken into account, especially on AMR. First, which particles lie within a given cell; and, second, which is the host cell of a specific particle. The Lagrangian map answers both questions. It is composed by a multi-level hash table that provides direct access to the ensemble of particles contained in each cell, as illustrated in Fig. (1), and it uses a per level search tool based on an algebraic equation to find the cell in which the particle lies within:

$$i_c = \text{int} \left(\frac{x_p - x_0}{\Delta x} \right), \quad j_c = \text{int} \left(\frac{y_p - y_0}{\Delta y} \right) \quad \text{e} \quad k_c = \text{int} \left(\frac{z_p - z_0}{\Delta z} \right), \quad (14)$$

where i_c , j_c e k_c are the Eulerian grid point index in the three coordinate directions, the coordinates x_0 , y_0 e z_0 correspond to the computational domain origin, Δx , Δy and Δz are

the local grid size and depends on the mesh level. This algorithm is $O(1)$ per level, as shown in Fig. (3).

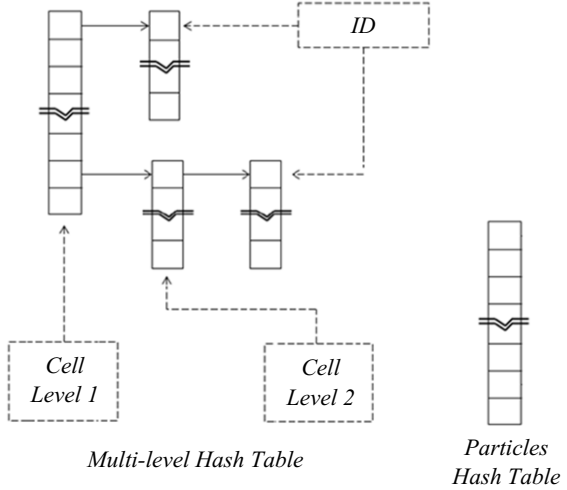


FIG. 1. Lagrangian map: computational model composed by a multi-level hash table of identifiers (ID) and a particles hash table.

Figure (1) shows that the first hash tables are always cell-type and the last one is always ID-type. The cells in which particles lie within are called *visible cells*. Since a multi-level hash table depends on Eulerian mesh, the code must rebuild its structure at each mesh refinement without losing any particle information.

The computational particles need to be represented in the code somehow. For this, it is used a hash table similar to the one used for the Lagrangian map. In this case, the hash table is of type ID, meaning that it consists on a list of indices that are the identifiers (IDs) of the particles and also the keys to access the information stored in the table. To obtain the properties of a specific particle, the only required information is its ID. From an ID, it is possible to access, through a hash function, all the other particle properties, as position, linear velocity, angular velocity, diameter, density, mass and others, without having to go through the entire table. Additionally, the table can hold n particles and their respective n variables, as shown in Fig (2).

The entire structure of the hash tables, applied both in the construction of the Lagrangian map and in the addition of particles and their properties, was employed in the MFSim code by means of the UTHASH package developed by [28] in C language. For this reason,

although the MFSim code is written in Fortran, the FDF module was developed in C. The UTHASH package provides tools to create and manipulate the tables in order to add, delete, and search for information contained in them.

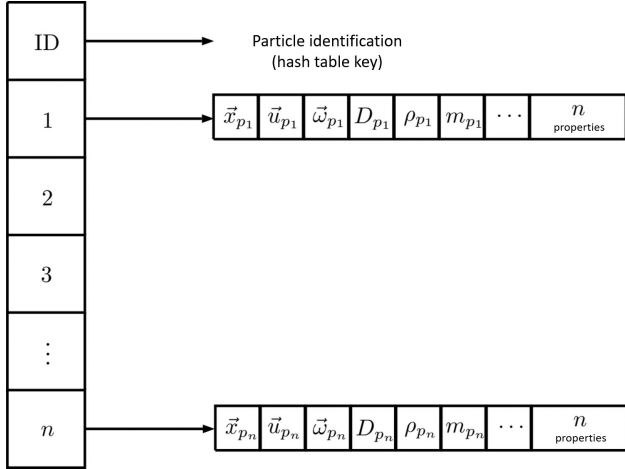


FIG. 2. Schematic representation of a has table used to store Lagrangian particles.

Figure (3) shows the search time for locating a particle on AMR using the Lagrangian map search tool. The horizontal axis represents the number of AMR levels, which corresponds to meshes from 512 up to one billion cells.

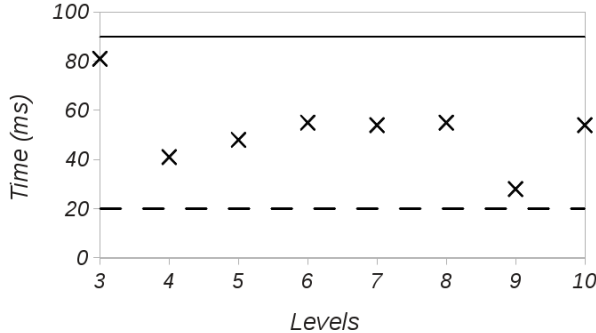


FIG. 3. Time, in milliseconds, for a random particle search using the Lagrangian map. The continuous and dashed line stand for the upper ($O(1)$) and lower bounds ($\Omega(1)$), respectively.

1. Particles initialization and transportation

The Lagrangian map structure is similar to a computational *tree*, i.e. visible cells in block-structured mesh are the *tree leaves*, as represented in Fig. (4). Visible cells distinguish

from the others because just the last layer of cells can hold particles.

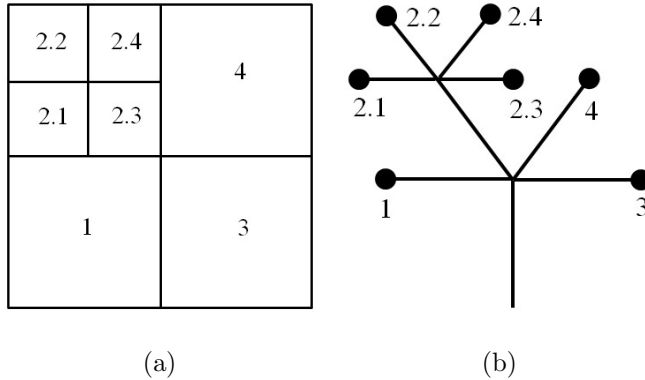


FIG. 4. (a) Two dimensions block-structured mesh. (b) Lagrangian map structure. The black discs represent the visible cells (leaves).

A recursive function to iterate the visible cells stored in the Lagrangian map is used. Once the algorithm finds these cells, it adds particle IDs using the stack. Each cell receives n identifiers, independently of its size and location in the flow domain. This approach is appropriate to Lagrangian FDF methods because it guarantees a homogeneous statistical cost throughout the computational domain.

The parallel transport of particles uses point-to-point and collective communication concepts of MPI. Initially, each process creates an *identifier / target process* list. Then, the root process gathers all lists and distributes them to the other processes. Finally, processes send and receive their particle's buffer, containing information such as position, weight and composition value.

IV. LAGRANGIAN COMPOSITION FDF CODE

A. MFSim code

The MFSim code is a computational framework able to solve monophasic and multiphasic turbulent flows using Lagrangian and Eulerian based numerical methods on an adaptive, block-structured mesh. It uses the Semi Backward Difference Formula (SBDF) method to discretize the filtered momentum transport equations respected to time. It treats the diffusive term implicitly and the advective term explicitly. For the discretization of the advective terms it is applied the Total Variation Diminishing method CUBISTA [38] and the

second-order Central Difference Scheme [29] to approximate diffusive terms of the transport equations. Scalar variables (e.g., pressure, density and viscosity) are located at the cell centre, and velocity components are stored on cell faces according to the staggered arrangement [39].

The flow variables (e.g., velocity and species mass fraction) evolve on an adaptive, block-structured mesh. The refinement criterion is based on properties gradients, such as the magnitude of the vorticity field, scalars and/or density field [24]. The resulting mesh is easily parallelized compared to unstructured mesh. Sene [40] discoursed on MFSim parallelization methods and used Message Passing Interface (MPI) [41 and 42] to communicate Eulerian based data among processes. The same approach is used to communicate Lagrangian information using the parallel Lagrangian map, as it will be seen in Section III A 1. The Multigrid technique, which employs the successive over-relaxation iterative solver to provide numerical solution for the Poisson equation, must be used because the diffusive terms of momentum equation are treated implicitly by the temporal discretization scheme.

A classical fractional step method [43] solves pressure and velocity separated and sequentially. Firstly, it determines an auxiliary filtered velocity \hat{u}_i field based on the filtered momentum transport equations, at this point without regards to mass conservation. Further, a Poisson equation provides an estimated filtered pressure $\langle q \rangle_\Delta$ based on the auxiliary filtered velocity field. Then, the method forces the auxiliary filtered velocity field to fit mass conservation, correcting \hat{u}_i with the estimated filtered pressure. After these steps, the filtered velocity field obeys mass conservation.

B. Lagrangian Monte Carlo algorithm numerical aspects

The LES and PDF solvers are coupled by means of a feedback mechanism that exchanges information at each integration time step. At the beginning of the simulations the flow field is initialized and the stochastic particles are uniformly distributed in the whole 3D Cartesian mesh. Balance equations for the mass and momentum are first solved within the Finite Volume (FV) framework. The filtered velocity components, the turbulence frequency and the diffusion coefficients are provided to the Lagrangian solver, so the particles evolution can be determined according to the stochastic differential equations. The filtered reaction rate term is evaluated using the Lagrangian representation, then it is fed to the Eulerian

progress variable transport equation. As a next step, the transport equation of the progress variable, is solved, so the temperature field is determined by means of Eq. (10), and the new density field is calculated from an equation of state. This procedure is repeated at each integration time step until the end of the simulations.

Some other numerical aspects are relevant to the use of the Lagrangian Monte Carlo method. This concerns, among others, the initialization of the particle field, the procedures of interpolation of the mean field variables to the particles, the particles weighting control and the mean values estimations are examples of those aspects, which will be addressed in the forthcoming paragraphs.

1. Treatment of initial and boundary conditions

Analogous to the situation in the Eulerian domain, where boundary conditions must be specified for solving the system of partial differential equations, boundary conditions must also be applied at the limits of the flow domain during a Monte Carlo simulation. The five most common types of boundary conditions are: outflow, inflow, symmetry, zero-flux wall and periodic conditions [3].

At an outflow boundary, the mean velocity vector points out of the flow domain. Thus, there is a net motion of particles in adjacent grid cells across the outflow boundary. In this case, these particles are simply eliminated. When symmetry boundaries or zero-flux-walls are the boundary conditions, particles may attempt to leave the flow domain across the boundary and the common procedure is to reflect these particles position back into the flow domain. Reflecting the particles does not change the particle composition (in the case of non-catalytic walls), but it may affect their temperature if the wall is non-adiabatic [44].

At an inflow boundary, the mean velocity vector points into the flow domain. Denoting the component of the mean velocity normal to the inflow surface (S_{in}) by U_{in} , then the total mass entering each computational volume at each time step Δt is:

$$\Delta m_{in} = \rho S_{in} U_{in} \Delta t. \quad (15)$$

The initial composition of the new particle must correspond to the inflow compositions. The initial position of particles in the physical space are randomly defined in directions Y and Z inside the finite volume cell of the inlet, and the position in X direction, based on the

Courant criteria, is evaluated as:

$$X^{(i)} = U_{in} \Delta t \xi, \quad (16)$$

where ξ is a random number ranging between 0 and 1.

If the flow of interest presents a temporal-evolving characteristic, such as the mixing flows studied in this work, periodic boundary conditions may be used. In this case, a particle that leaves the computational domain is automatically added at its opposite (inflow) direction, naturally taking into account the distance traveled near and after leaving the outflow boundary.

2. Initialization of the particle field

The number of particles within each control volume is prescribed to be initially uniform. However, a given stochastic weight, evaluated through Eq. (15), is attributed to the particles in such a manner that the particle mass and density fields are consistent with the finite-volume mass and density values. The particles initial positions are randomly distributed within each control volume, despite the level of refinement of where it is positioned, and the associated properties, such as scalar values, are also prescribed consistent with the corresponding Eulerian initial values.

3. Interpolation of average Eulerian quantities to the particle field

In order to model the particles transport in the physical space, it is necessary to interpolate the mean velocity field, given by the LES simulation, to the particles positions. This is accomplished by, first, interpolating the velocities from the control volume faces to the nodes of the finite-volume grid. Once the velocity components at each node of a given control volume are known, a method of interpolation based on the distance weighting is used to interpolate the velocities components from the nodes to the particles positions [45].

In this interpolation method, the velocity of a particle that lies within a control volume is weighted by the inverse of the square of the distance between the particle and the nodes, i.e:

$$\hat{u}_{ip} = \frac{\sum_{No=1}^8 (\tilde{u}_{i,No}/\mathcal{D}_{No})}{\sum_{No=1}^8 (1/\mathcal{D}_{No})}, \quad (17)$$

where \tilde{u}_{ip} is the i -th component, $i = 1, 2, 3$, of the velocity vector interpolated at the particle p , $No = 1, \dots, 8$ is an index associated to a node in a finite-volume hexahedral grid, and \mathcal{D}_{No} is the square of the distance between the particle and a node No , that is given by:

$$\mathcal{D}_{No} = (x_p - x_{No})^2 + (y_p - y_{No})^2 + (z_p - z_{No})^2, \quad (18)$$

where x_p , y_p and z_p are the coordinates of a particle p in the x , y and z directions, respectively, and x_{No} , y_{No} and z_{No} are the positions of the nodes of the considered control volumes. The nodes No distances \mathcal{D}_{No} and the particle p are illustrated in the Fig. (5).

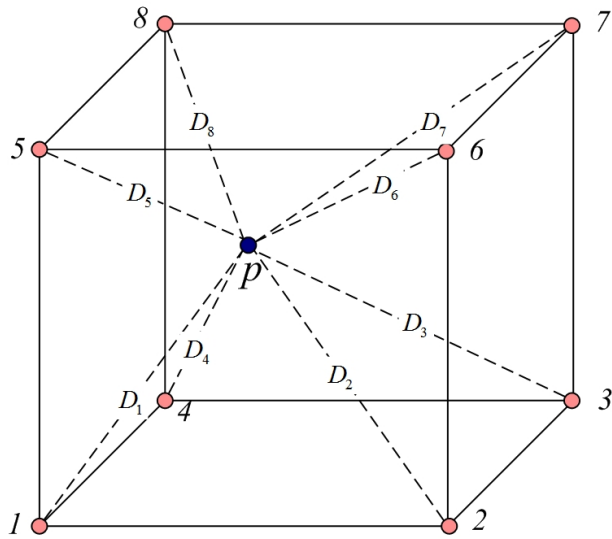


FIG. 5. Weighted interpolation scheme. The solid lines represent the control volume edges, and the dashed lines connects the nodes and a particle p .

4. Estimation of average quantities from particle fields

A fundamental issue in hybrid Monte Carlo-Finite Volume methods is the estimation of average quantities from noisy data. In the present research, this issue happens for properties such as the chemical reaction progress variable, the density and the chemical reaction rate evaluated at each particle. The mean values of the last two quantities are directly used in the transport equations. Since each particle has its own mass, it is natural to use an average weighted by the mass of the particles. Considering a Lagrangian property Q , the weighted

average $\langle Q \rangle$ in a given control volume n is given by:

$$\langle Q \rangle_n = \frac{\sum_{l=1}^{N_p^n} m^{(l)} Q}{\sum_{l=1}^{N_p^n} m^{(l)}}, \quad (19)$$

where N_p^n is the total number of particles in a given control volume n , and $m^{(l)}$ is the mass of each particle l .

C. Particle population control

Due to the stochastic nature of the method of Monte-Carlo and the turbulent motions, the number of particles present in a given cell may significantly change in time. As it can be derived for constant density flows, the average number of particles per cell is proportional to the cell volume if all particle masses are equal [3]. In order to prevent particle accumulations, particles are ascribed a relative weight, which may vary throughout the computational domain and even among the particles within a single computational cell [46]. The particles evolve in such a manner that the evolution of the joint FDF is equivalent to the FDF in the physical transport equation. The stochastic particles, therefore, do not need necessarily to behave as fluid particles, i.e., they can have mass, but not inertia. In fact, each of them represents a single realization of the turbulent flow [47]. It is worthy to recall that the number of stochastic particles per cell is a crucial issue for the developments of this work, since the error of the method decays with the order of $1/\sqrt{N_p}$, where N_p is the number of particles retained.

To maintain an acceptable distribution of particles as they move in physical space, particle *cloning* and *annihilation* algorithms are employed [46]. Particles are cloned in control volumes having less particles than a pre-determined value by splitting a particle of mass m into two particles, each one with mass $m/2$ and maintaining the same properties as the original particle. Thus, the highest-mass particles in each element may be cloned. Haworth [22] argues that cloning does not modify the local PDF of particle properties. However, as demonstrated in [39], in the context of variable density flows using a conserved scalar, as the chemical reaction progress variable, choosing the highest-mass particles, as suggested by [22], may shift inadvertently the local PDF, changing the local mixture composition. This happens because the highest-mass particles are usually the particles representing fresh gases, due to their lower density.

Damasceno, Santos and Vedovoto [39] developed an algorithm of particle density control that is implemented in a way that, even when the number of notional particles drastically changes inside a control volume, no information about the subgrid is lost, since the original shape of the PDF may be recovered. This is particularly suitable for AMR computations because, during operations of refining the local mesh, the number of notional particles per control volume must be kept within the tolerance criterion. As a consequence, this implies in creating 8 times the number of particles originally positioned on a coarser level, since, in a 3D domain, each coarse cell originates eight finer cells. When a coarsening procedure is necessary, notional particle population reductions of the order of 87.5%, or a reduction of the local population of 8:1, are a common operation. Naturally, the algorithm implemented conserves at least second-order statistical quantities, ensuring mass, mean values and variance. In the best scenario, when the number of particles is reasonably high enough to evaluate a probability density function, its shape may be recovered. The algorithm is fully adapted in the in-house code MFSim.

V. RESULTS

The main objective of this section, in concordance with the aim of the present work, is to demonstrate the capabilities of the recently implemented LES-AMR-FDF transported method coupling, and not to solve yet any industrial engineering problem. However, even though industrial application is out of the scope of this paper, this kind of problems is envisaged for future works.

A. Partially Stirred Reactor

The Partially Stirred Reactor (PaSR) simulation consists in calculating the effect of molecular diffusion over an initially segregated fluid using a micromixing model. For industrial applications, one may model chemical reactors as PaSR. In CFD simulations that apply Lagrangian composition FDF method, each cell is a PaSR. To contextualize the CFD application of PaSR, the chemical reactor and some mathematical models are presented. After, simulation results for a cubic PaSR using the Interaction by Exchange with the Mean (IEM) micromixing model [21, 48, and 49] are showed.

It is possible to model a Perfectly Stirred Reactor (PSR), to which the hypothesis of fluid homogeneity applies. This hypothesis is based on the intense turbulent mixture inside the reactor. The PSR is not dependent on micromixing (i.e., the effect of molecular diffusion on mixture), but just on fluid residence time. The assumption of PSR is not satisfied when the turbulent mixing rate is smaller than the chemical reaction rate, considering that the model becomes inaccurate to predict flow variables.

1. *PaSR simulation*

The PaSR simulation is performed in a cubic box, which is filled with notional particles that evolve in Cartesian and composition spaces, as expressed by Eqs. (7) and (8). The composition value of each particle is initialized by a hyperbolic tangent function, with the objective of initially segregating the particles through its scalar value [27]:

$$\zeta(y) = \frac{\zeta_1 + \zeta_2}{2} + \frac{\zeta_1 - \zeta_2}{2} \tanh\left(\frac{2y}{\delta_m} - \frac{2h_m}{\delta_m}\right), \quad (20)$$

where y is the box height coordinate, ζ_1 and ζ_2 are the initial composition values, δ_m is the initial mixture width and h_m is the coordinate where mixture initially occurs.

The Probability Density Function (PDF) has a wide usage in FDF methods that predict the value of SGS random variables in mixing and reactive flows [26]. The PDF is useful to analyze central moments (e.g., average) and distribution moments (e.g., variance) of a random variable, since these moments are integral functions of it. Here, the variable ζ describes an Eulerian composition field computed based on particles mean $\overline{\phi^*}$, and ϕ^* stands for a particle composition value.

In the Lagrangian approach, each notional particle assumes a value between ϕ_{max}^* and ϕ_{min}^* . Therefore, this range can be discretized to count the number of particles that match each sub-range and further build the so-called empirical PDF.

Fig. (6) presents the empirical PDF evolution in PaSR at three times: 0, 200 and 1000 s. The initial shape of double delta function (continuous line) tends to a single delta function at the global mean $\overline{\phi^*} \approx 0.45$ (dotted line). As the composition variance reduces, micromixing occurs [3], as it can be seen in the right-hand side of Fig. (6).

The fact that the IEM model leads the scalar variable to relax toward to the average value, without, however, accounting for scalar gradients, is exemplified in Fig. (6-a). In this

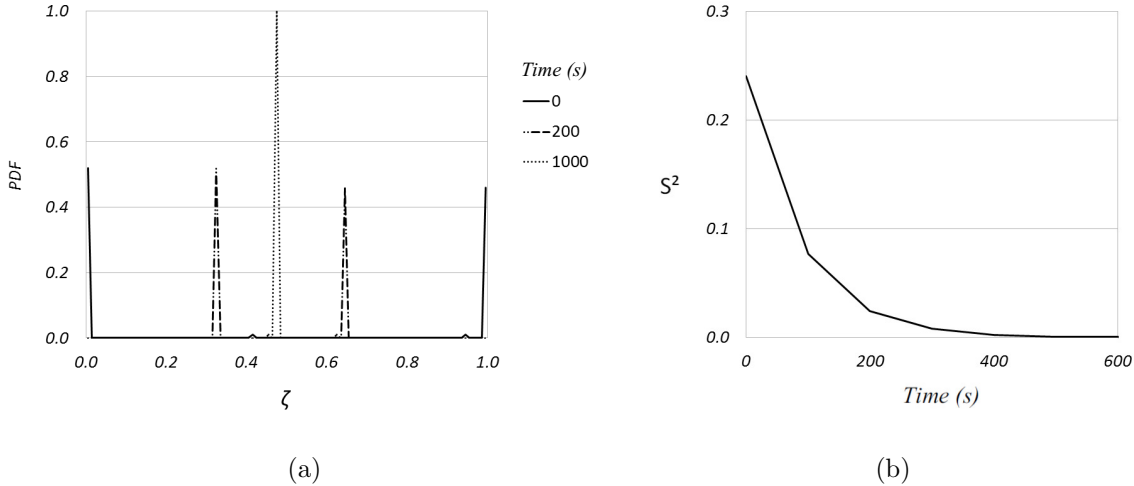


FIG. 6. PDF evolution and consequent variance decay. (a) Empirical composition PDF during PaSR simulation and (b) Composition variance during PaSR simulation

figure, the shape of the scalar PDF is shown for different discrete times. At $t = 0$, it can be noted that the PDF exhibits two peaks along the c axis, around zero, and one. These two peaks correspond to a probability of 50% of particles with $c = 0$ and 50% of particles with $c = 1$. Again, as time evolves, the distance between the two peaks begins to decrease and the probability of having particles with intermediate values of c between 0 and 1 increases, indicating that the mixing is over the particles, forcing the values of all particles to tend towards 0.5, and, finally, the probability to obtain this values achieves 100%.

B. Statistical equivalence between Eulerian and Lagrangian approaches

In this section, it is presented the verification of a fundamental pre-requisite of a hybrid LES-FDF method, the equivalence between the Eulerian and Lagrangian approaches. The model of transported PDF retained in the present work is based on the hypothesis that the stochastic differential equations, Eqs. (7) and (8), give statistically equivalent results to the solution of the Eulerian equation of transport of the scalar field PDF, Eqs. (12) and (13), respectively, when solved over a sufficient large number of Lagrangian particles using the Monte Carlo method.

In this sense, a requirement for the use of the transported PDF model, coupled with a finite-volume model, is the verification of the statistical equivalence between the two approaches, based on Eulerian and Lagrangian referentials, respectively. The verification

procedure is performed by simulating non-reactive cases, where statistical central moments of first and second orders are evaluated and compared quantitatively using both approaches. Another important verification test performed is to ensure the consistency, i.e., the distribution of particle mass in physical space is not arbitrary and it must remain consistent with the fluid mass, or volume, distribution.

A general idea to ensure mass conservation is to devise a system of *notional* particles whose evolution yields the same one-point and one-time PDF as the real fluid particle system [22]. Each notional particle represents a specified mass of fluid $m^{(i)}$, given by Eq. (15), of an assembly of N_p particles. The expected value of the mass of particles in each finite-volume cell should be equal to the mass of fluid in the finite volume cell. The mass of fluid in a finite-volume cell of volume V_c is $m_{FV} = \bar{\rho}V_c$, and the mass of particles in that same volume is $m_{pc} = \sum_{n=1}^{N_{pc}} m^{(n)}$, where the sum applies over all particles in the cell. Thus, the requirement is: $\langle m_{pc} \rangle = m_{FV}$. The rules associated with the particle *cloning* and *annihilation* algorithms are used precisely for ensuring mass conservation.

To demonstrate the equivalence between the Eulerian and Lagrangian schemes in variable density flows, a temporal mixing layer involving the transport of a passive scalar quantity c featuring increasing values of the density ratio is studied. The modeling equations for such a variable are the same transport equations that govern the chemical reaction progress variable. However, it is important to note that in the present section there is no chemical reaction. The flow configuration consists of two co-flowing streams travelling in opposite directions with the same reference velocity $U_r = \Delta U/2$, where ΔU denotes the velocity difference across the layer.

The flow variables reported below are normalized with respect to a reference length scale L_r equal to half the initial vorticity thickness, i.e., $L_r = \delta_v(t=0)/2$. The corresponding flow is dominated by the growth of large scale coherent Kelvin Helmholtz type structures. In the retained representation, x and y denote the streamwise and the cross-stream directions, respectively. The temporal mixing layers are initiated by a hyperbolic-tangent velocity profile, i.e., $u = U_r \tanh(y/L_r)$, with free stream conditions, as $u_1 = U_r = 1$ and $\phi_1 = 1$ at the top, and $u_2 = -U_r = -1$ and $\phi_2 = 0$ at the bottom. A weak white noise random perturbation is superimposed on the initial velocity field in the rotational region. Simulations are conducted at $Re = U_r L_r / \nu = 5000$ for four different values of the density ratio $s = 1$ and $s = 6$, where s is the characteristic density contrast defined as $s = \rho_1/\rho_2$. $\rho_1 = \rho(c_1)$

and $\rho_2 = \rho(c_2)$ denote the values of the density in the top and bottom streams, respectively.

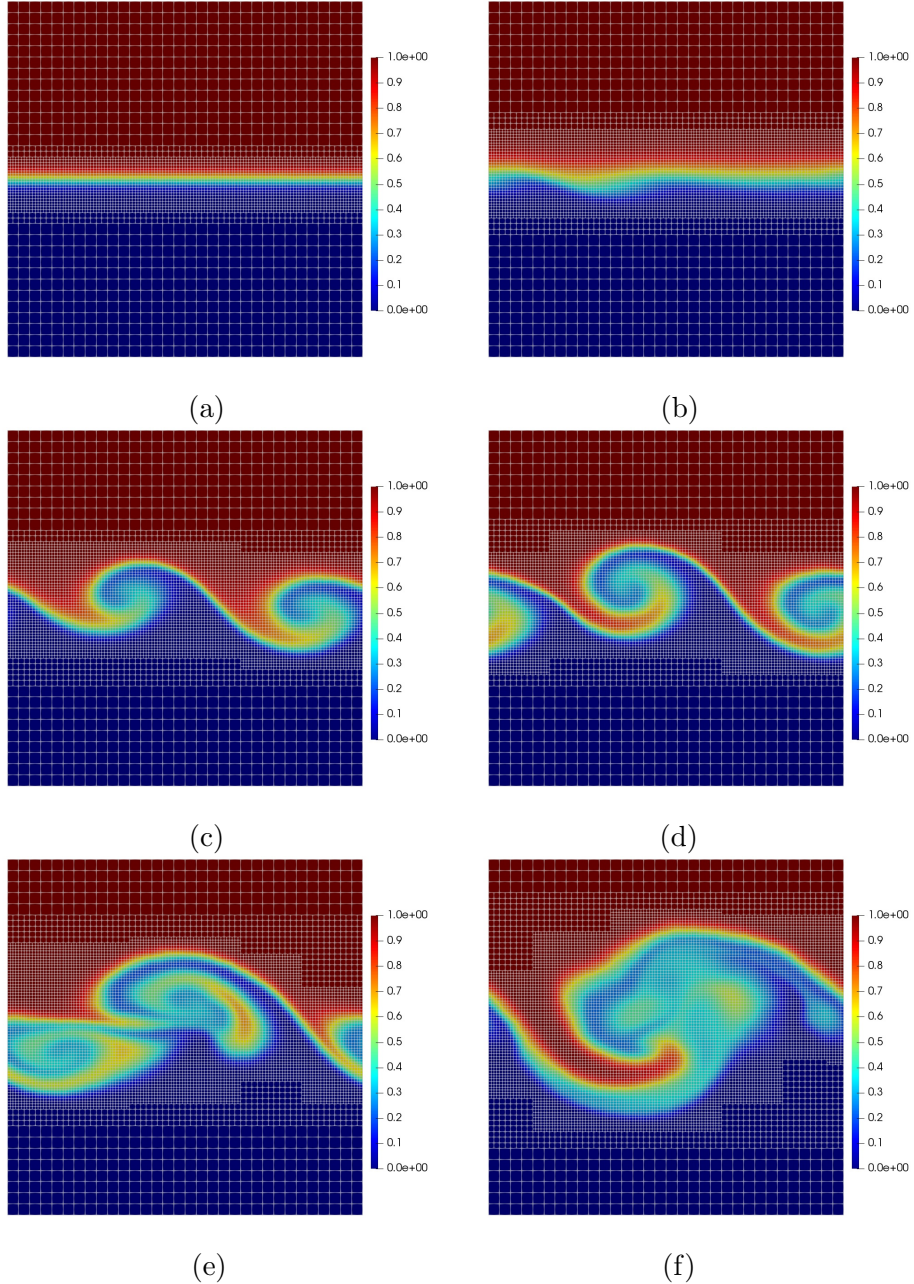


FIG. 7. Instantaneous snapshots at medium plane in Y direction showing the mesh adaptation accordingly to the gradient of c evaluated from the Lagrangian FDF code. (a) $t=0.0\text{s}$, (b) $t=0.54\text{s}$, (c) $t=1.08\text{s}$, (d) $t=1.62\text{s}$, (e) $t=2.16\text{s}$ and (f) $t=2.7\text{s}$

Three levels of refinement are used, with a bottom level of $32 \times 8 \times 32$ control vol-

umes in each coordinate direction (x , y and z , respectively), which means that in the top level, the most refined one, the computational mesh features a local refinement equivalent to $128 \times 32 \times 128$ control volumes. It is noteworthy that the grid spacing in each level is constant. For all simulations presented in this subsection, the time step size is allowed to be variable. However, the security factor that controls the time step calculation, namely the Courant-Friedrichs-Lowy (CFL) criterion, is fixed in 0.1. Concerning the Monte-Carlo approach, the simulations are carried out retaining $N_p = 25$ particles per control volume. Since the grid is dynamically adaptive, as a criterion for mesh adaptation, vorticity and gradient of \tilde{c} are chosen. The adaptation of the grid with time can be verified in Fig. (7). As boundary conditions for the Eulerian approach, periodic boundary conditions are applied in x and y coordinate directions. For the momentum equation, Dirichlet boundary conditions are used at top and bottom walls. For the chemical reaction progress variable and its variance, zero-flux boundary are applied at those walls. Concerning the Lagrangian framework, the periodic boundary condition is also applied, and, for the top and bottom walls, specular reflection is adopted.

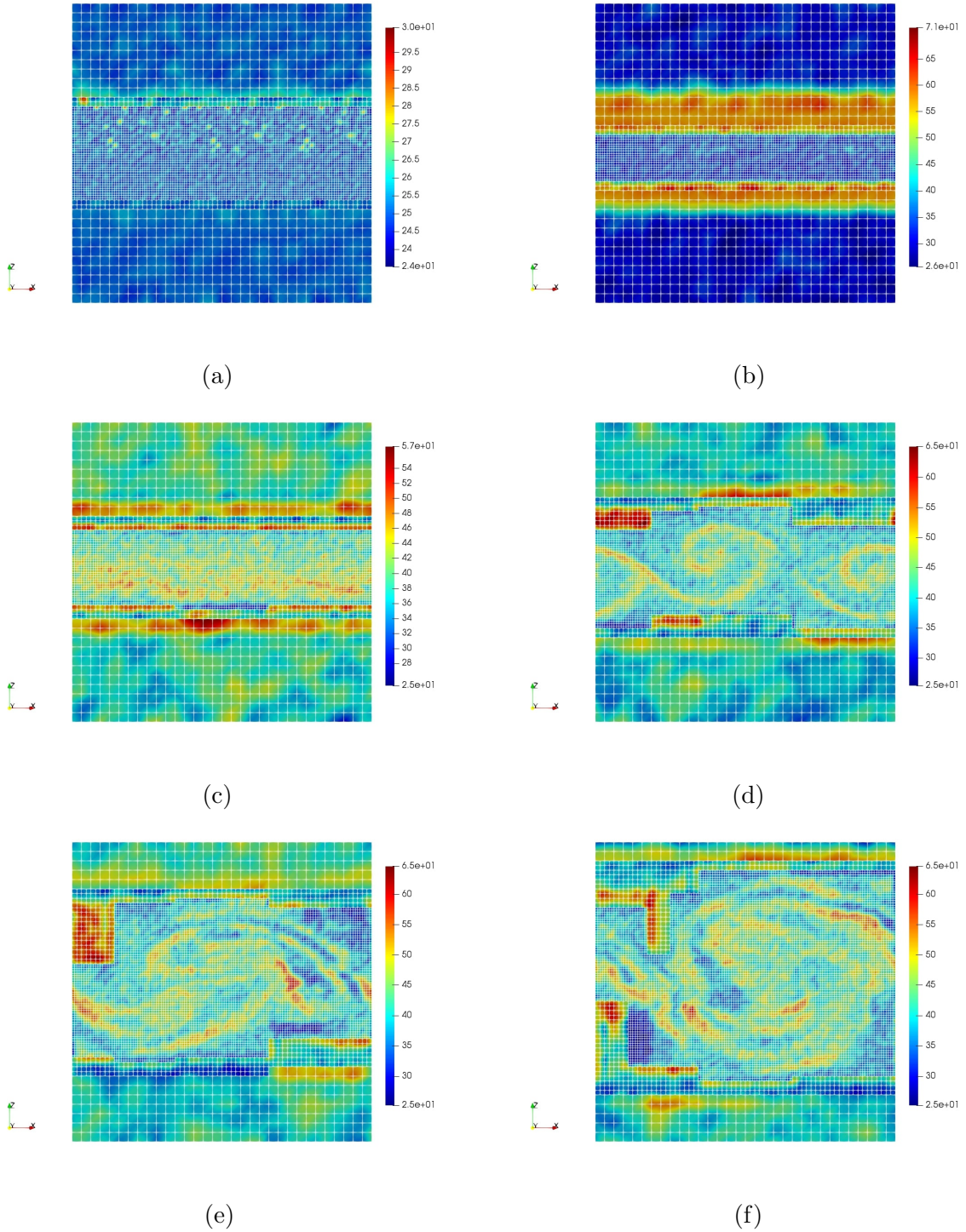


FIG. 8. Instantaneous snapshots at medium plane in Y direction displaying the number of notional particles per control volume. (a) $t=0.0\text{s}$, (b) $t=0.54\text{s}$, (c) $t=1.08\text{s}$, (d) $t=1.62\text{s}$, (e) $t=2.16\text{s}$ and (f) $t=2.7\text{s}$

Since the accuracy of the Monte-Carlo method depends directly on the number of particles in a given computational cell, in the present work, the cloning and annihilation algorithms act only where the number of particles is 80% smaller or 3 times higher than the initial number of particles. The effects of such limits are clear during the processes of grid adaptation. Figs. (8) (a) to (f) show the evolution of a temporal mixing layer, where $s = 6$ and $C_\omega = 2$. The computational setup retained are the same for Figs. (7) and (8).

It is interesting to note the behavior of the number of notional particles per control volume. It can be seen in Fig. (8) that, from the initial configuration until $t = 0.54\text{ s}$, the layer of refined mesh diminished, keeping refined grids closer to the shear layer. In the upper part, a quick increase in the number of particles can be noted (the scale limits are adjusted to the maximum and minimum values of the property in each sub-figure). In principle, the number of particles per control volume should be around N_p . However, one must keep in mind that during the process of coarsening a control volume, eight smaller cells should become just one coarser cell. Hence, if originally the sum of particles in those eight cells are supposed to be 200 (8 cells times N_p each), after the remeshing procedure a reduction of 87.5% in the local notional particles population is needed. Finally, since the upper limit established for the simulations is three times N_p , the number notional particles should be around $3 \times N_p$, or, in the present work, around 75 notional particles in a recently coarsened region, as it can be evidenced.

As time evolves, both the dynamics of fluid motions and the stochastic nature of the Lagrangian FDF model are responsible for the mixing of these newly generated particles. It is worth noting that following the procedure presented in [39], during the cloning and annihilation procedures, statistical moments up to the second are conserved.

Figs. (9) and (10) show the comparisons of mean values of the property ϕ and its variance, both evaluated in Eulerian and Lagrangian referentials. Here, the simulation is carried out using $s = 1$ and $C_\omega = 2$. The remaining computational and physical setup is the same as the previously presented. It can be noted that qualitatively the Eulerian and Lagrangian fields present a remarkable similarity. In order to verify quantitatively such a similarity, linear probes along X and Z directions, at $Z = L_r/2$ and $X = L_r/2$, respectively, are extracted. For the same conditions previously presented, an assessment of the Euler-Lagrange equivalency dependency on N_p is performed. Four different values of N_p are used, 25, 50, 100 and 200, and the results are shown in Fig. (11).

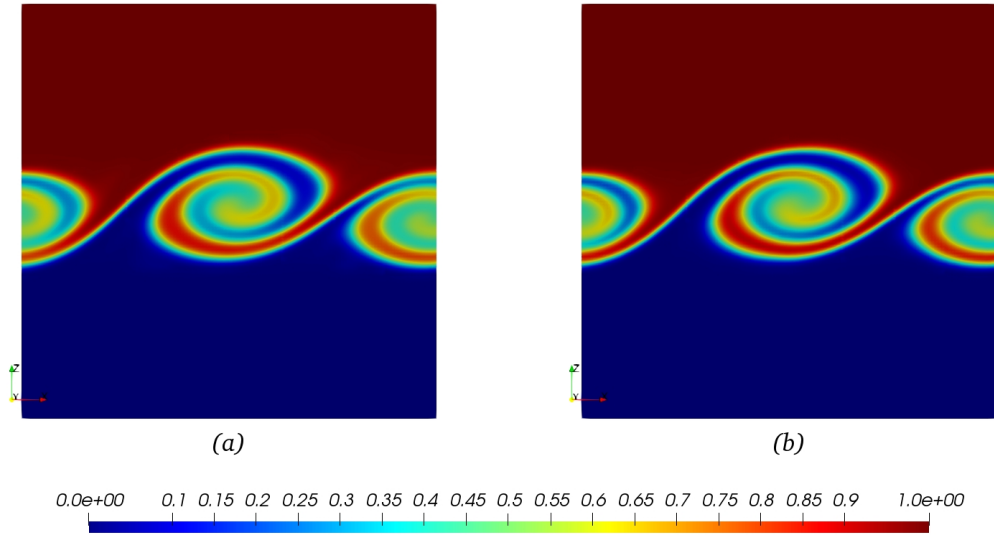


FIG. 9. Mean values of the progress variable \tilde{c} . (a) Finite Volume Method and (b) Lagrangian FDF method for $t = 1.811\text{ s}$. Three levels of refinement with $N_p = 200$ were used.

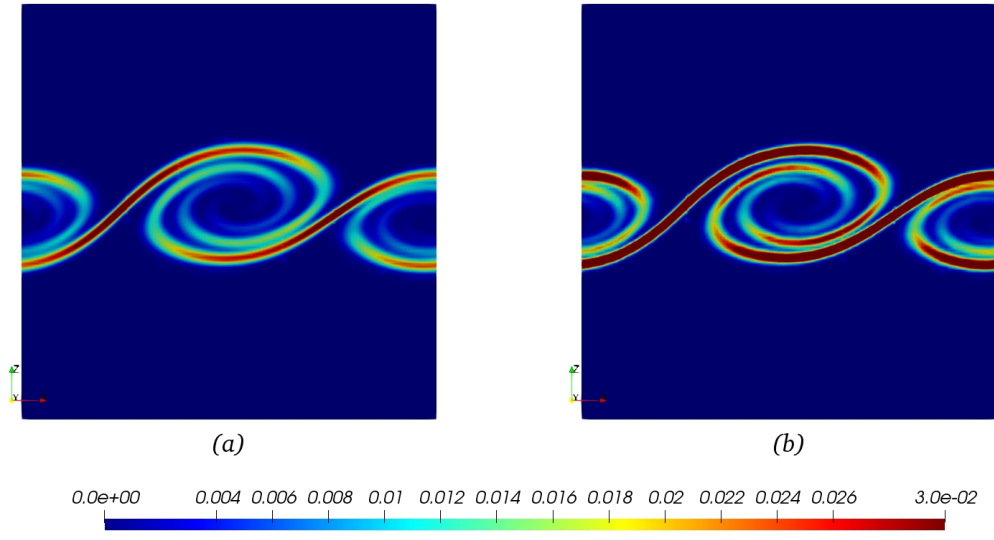


FIG. 10. Mean values of the progress variable variance \tilde{c}^2 . (a) Finite Volume Method and (b) Lagrangian FDF method for $t = 1.811\text{ s}$. Three levels of refinement with $N_p = 200$ were used.

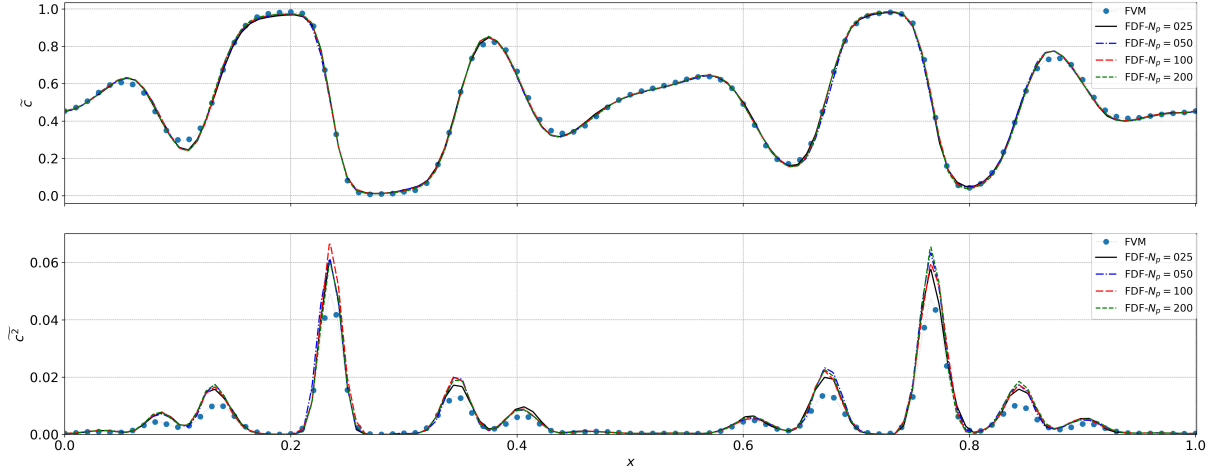


FIG. 11. Mean values of ϕ and its variance evaluated in both Eulerian and Lagrangian frameworks. Linear probes along Z and X directions.

It can be noted in Fig. (11) that there is virtually no dependency on N_p , and that the statistical equivalence of the variance does not agree very well. In order to verify if such discrepancy is due to the Eulerian refinement, one level of refinement is added. Figs. (12) and (13) display instantaneous comparisons of the progress variable \tilde{c} and its variance $\tilde{c''}^2$ at $t = 1.7478\text{ s}$. The results of linear probes confirming the Euler-Lagrange statistical equivalence are shown in Fig. (15).

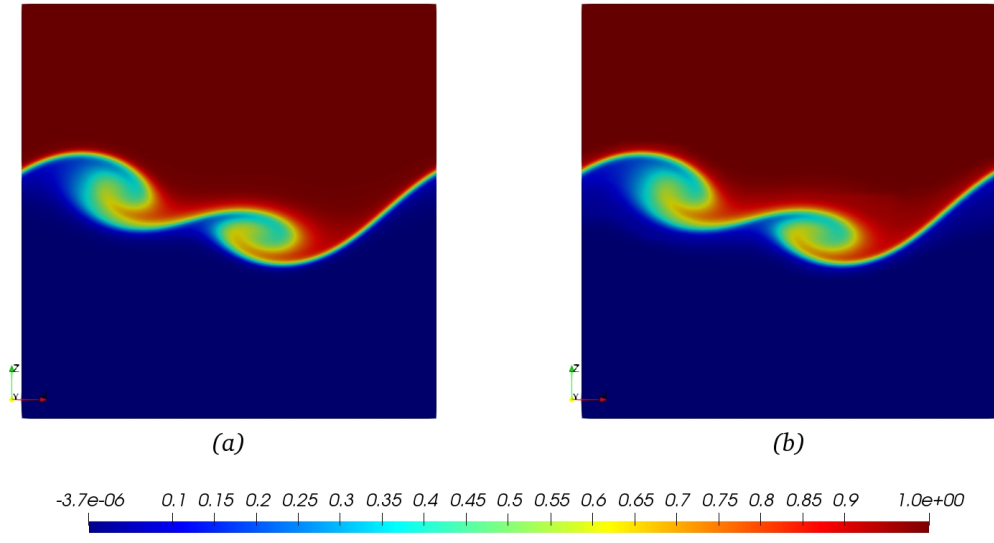


FIG. 12. Mean values of the progress variable \tilde{c} . (a) Finite Volume Method and (b) Lagrangian FDF method for $t = 1.7478$ s. Four levels of refinement with $N_p = 100$ were used.

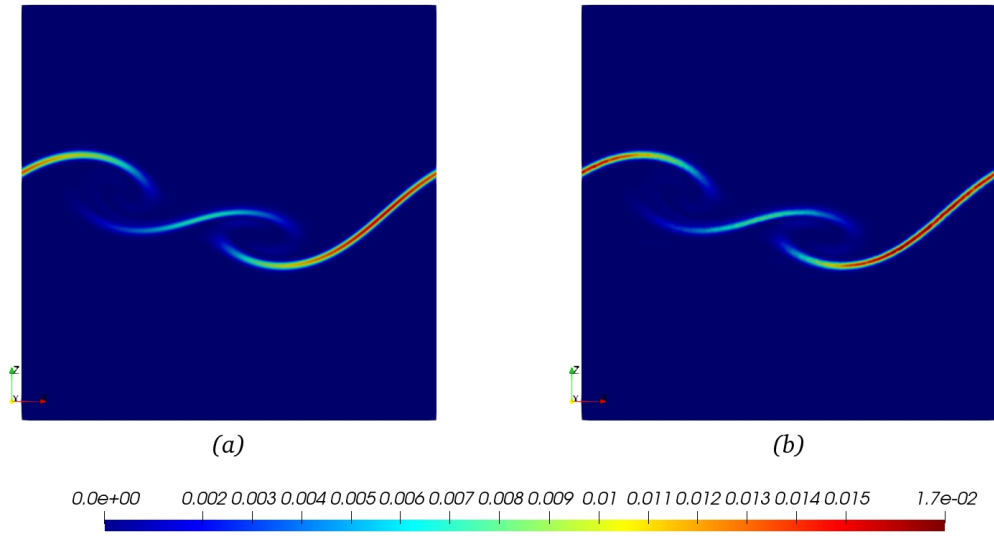


FIG. 13. Mean values of the progress variable variance \tilde{c}^2 . (a) Finite Volume Method and (b) Lagrangian FDF method for $t = 1.7478$ s. Four levels of refinement with $N_p = 100$ were used.

It is noteworthy the effect of the refinement level in the statistical equivalence of the Eulerian and Lagrangian approaches. In the simulation presented in Figs. (12), (13) and (15), four levels of refinement are used. As for refinement criteria, it is used once again

the vorticity and the gradient of \tilde{c} . However, in this case, the finest grid achieved a local resolution of $256 \times 64 \times 256$ control volumes in each coordinate direction, which means a much more accurate prediction of the shear layer position.

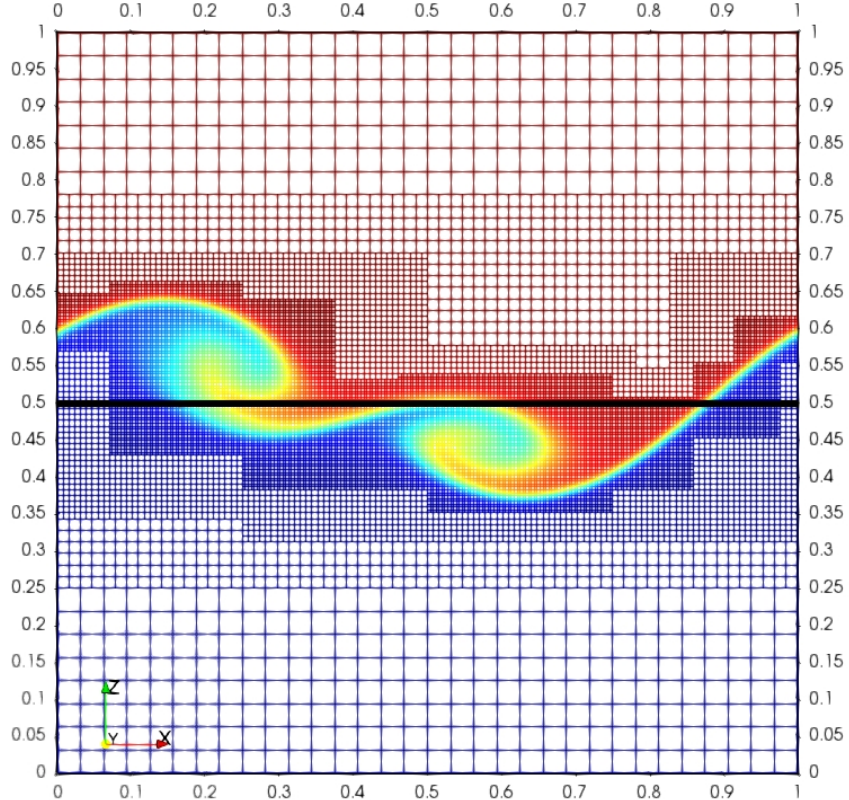


FIG. 14. Adaptive grid colored by progress variable \tilde{c} at $t = 1.7478\text{ s}$. The solid black line marks the probe position along the x-axis.

In Fig. (14) it is displayed the position of a linear probe used to verify the equivalence between the Eulerian and Lagrangian approaches in the simulation of a temporally evolving mixing layer. It can be noted that the probe is located starting from coordinate $Z = 0.5\text{ m}$, it passes through a small region with three levels of refinement. It can be verified in Fig. (15) that only from 0.75 to 0.9 in X direction appears a slightly difference between Eulerian and Lagrangian approaches regarding the mean value of \tilde{c} .

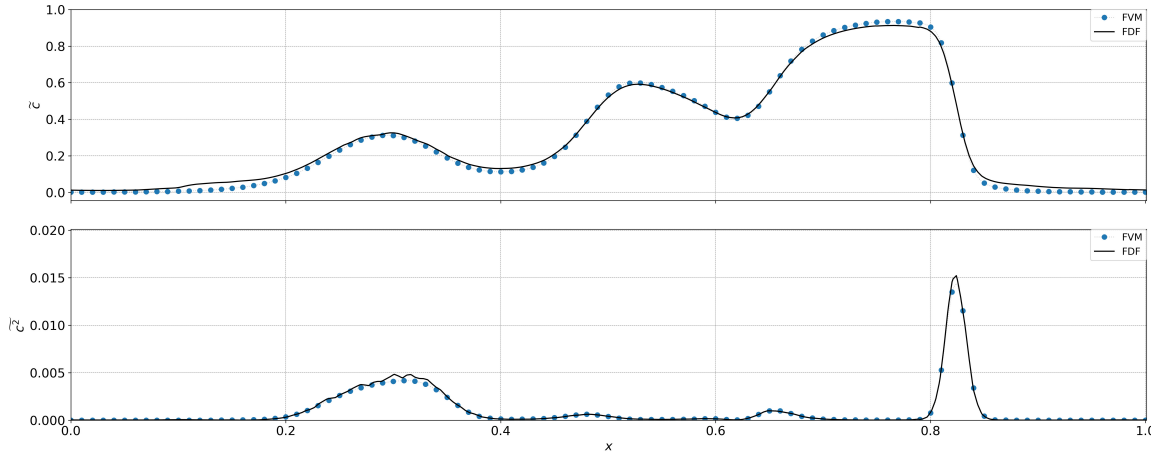


FIG. 15. Linear probes along X direction for the simulation with four levels of refinement and $N_p = 100$. Top figure: Chemical reaction progress variable \tilde{c} , and its variance in the bottom figure. Instantaneous probe taken at $t = 1.5170$ s

The simulation of a temporal mixing layer with four levels of refinement and $N_p = 100$ highlights one of the most powerful characteristics of the methodology presented in this paper. If one considers a full resolved computational domain, with a regular grid retaining the same level of refinement exhibited in the top-level, i.e. $256 \times 64 \times 256$ grid points, it would yield approximately 850 millions of notional particles, which represents quite a cumbersome computational cost. With AMR, on the other hand, the number of particles is about 150 million, about 5.6 times less particles, with no loss in accuracy in regions of interest, such as high gradient regions.

Finally, despite the differences between the numerical algorithms retained for the transport of a single passive scalar, in either constant or variable density flows, both the Eulerian and the Lagrangian fields agree very well and feature negligible differences. This confirms, at least, that the transport equations for the scalar are well implemented, ensure mass conservation and evaluate satisfactorily the first two central statistical moments.

VI. CONCLUDING REMARKS

A hybrid LES / Lagrangian FDF method on adaptive, block-structured mesh is implemented. This method has a potential to simulate the physics of multiple-species, turbulent

mixing flows with chemical reaction and combustion, using the LES approach and modeling the subgrid composition fluctuations in a probabilistic manner with the great advantage of directly integrating the chemical reaction rate. A Monte Carlo technique on an adaptive, block-structured mesh is developed. This involves notional particles normalization and comprehends the processes of cloning, guaranteeing a bounded Monte Carlo accuracy and maintaining the numerical error homogeneously distributed throughout the flow domain, and annihilation, preventing computer memory to overload.

In order to evaluated the methodology here proposed, numerical simulations of laminar and turbulent mixing flows are performed to check the stochastic method consistency. Finally, to the best knowledge of the authors, the use of Lagrangian FDF modeling on a dynamically adaptive mesh refinement environment is a novelty. Since one of the most acknowledged drawbacks of particle-based methods is its high computational cost, the resort to AMR reduced drastically the computational cost, with no loss of accuracy.

ACKNOWLEDGMENTS

The authors would like to thank PROPP-UFU, CNPq, CAPES, FAPEMIG and PETRO-BRAS S.A. for the financial and material support.

DATA AVAILABILITY

The data that support the findings of this study are available from the corresponding author upon reasonable request.

REFERENCES

- ¹M. Germano, U. Piomelli, P. Moin, and W. H. Cabot, “A dynamic subgrid-scale eddy viscosity model,” Physics of Fluids A: Fluid Dynamics **3**, 1760 – 1765 (1991).
- ²P. J. Colucci, F. a. Jaberi, P. Givi, and S. B. Pope, “Filtered density function for large eddy simulation of turbulent reacting flows,” Physics of Fluids **10**, 499 (1998).
- ³R. O. Fox, *Computational Models for Turbulent Reacting Flows* (Cambridge University Press, 2003).
- ⁴H. Aghakhani and A. K. Patra, “Scalable discrete adjoint for the transient savage–hutter

equation on the primal consistent adaptive grid,” *Engineering with Computers* **35**, 1251–1268 (2019).

⁵M. Cai, A. Nonaka, J. B. Bell, B. E. Griffith, and A. Donev, “Efficient variable-coefficient finite-volume stokes solvers,” *Communications in Computational Physics* **16**, 12631297 (2014).

⁶J. Cervený, V. Dobrev, and T. V. Kolev, “Non-conforming mesh refinement for high-order finite elements,” *CoRR* **abs/1905.04033** (2019), arXiv:1905.04033.

⁷F. Hecht, “New development in freefem++,” *J. Numer. Math.* **20**, 251–265 (2012).

⁸N. A. Simakov, R. L. Jones-Ivey, A. Akhavan-Safaei, H. Aghakhani, M. D. Jones, and A. K. Patra, “Modernizing titan2d, a parallel amr geophysical flow code to support multiple rheologies and extendability,” in *High Performance Computing*, edited by M. Weiland, G. Juckeland, S. Alam, and H. Jagode (Springer International Publishing, Cham, 2019) pp. 101–112.

⁹M. P. Katz, A. Almgren, M. B. Sazo, K. Eiden, K. Gott, A. Harpole, J. M. Sexton, D. E. Willcox, W. Zhang, and M. Zingale, “Preparing nuclear astrophysics for exascale,” in *SC20: International Conference for High Performance Computing, Networking, Storage and Analysis* (2020) pp. 1–12.

¹⁰N. Ansari, G. M. Goldin, M. R. H. Sheikhi, and P. Givi, “Filtered density function simulator on unstructured meshes,” *Journal of Computational Physics* **230**, 7132 – 7150 (2011).

¹¹A. Dubey, K. Antypas, and C. Daley, “Parallel algorithms for moving lagrangian data on block structured eulerian meshes,” *Parallel Computing* **37**, 101 – 113 (2011).

¹²M. J. Berger and J. Oliger, “Adaptive mesh refinement for hyperbolic partial differential equations,” *Journal of Computational Physics* **53**, 484–512 (1984).

¹³M. J. Berger and A. Jameson, “Automatic adaptive grid refinement for the euler equations,” *AIAA Journal* **23**, 561–568 (1985).

¹⁴S. Quan and D. P. Schmidt, “A moving mesh interface tracking method for 3d incompressible two-phase flows,” *Journal of Computational Physics* **221**, 761–780 (2007).

¹⁵P. T. Bauman and R. H. Stogner, “Grins: A multiphysics framework based on the libmesh finite element library,” *SIAM Journal on Scientific Computing* **38**, S78–S100 (2016).

¹⁶M. Pivello, M. Villar, R. Serfaty, A. Roma, and A. Silveira-Neto, “A fully adaptive front tracking method for the simulation of two phase flows,” *International Journal of Multiphase*

Flow **58**, 72 – 82 (2014).

¹⁷H. Samet, *The Design and Analysis of Spatial Data Structures* (Addison-Wesley Longman Publishing Co., Inc., USA, 1990).

¹⁸S. Popinet, “Gerris: a tree-based adaptive solver for the incompressible euler equations in complex geometries,” Journal of Computational Physics **190**, 572–600 (2003).

¹⁹M. Berger and I. Rigoutsos, “An algorithm for point clustering and grid generation,” IEEE Transactions on Systems, Man, and Cybernetics **21**, 1278–1286 (1991).

²⁰M. Berger and P. Colella, “Local adaptive mesh refinement for shock hydrodynamics,” Journal of Computational Physics **82**, 64–84 (1989).

²¹S. Pope, *Turbulent Flows*, Vol. 1 (Cambridge University Press, New York, 2000).

²²D. Haworth, “Progress in probability density function methods for turbulent reacting flows,” Progress in Energy and Combustion Science **36**, 168–259 (2010).

²³H. D. Ceniceros, A. M. Roma, A. Silveira-Neto, and M. M. Villar, “A robust, fully adaptive hybrid level-set/front-tracking method for two-phase flows with an accurate surface tension computation,” Communications in Computational Physics **8**, 51–94 (2010).

²⁴F. Denner, D. R. van der Heul, G. T. Oud, M. M. Villar, A. da Silveira Neto, and B. G. van Wachem, “Comparative study of mass-conserving interface capturing frameworks for two-phase flows with surface tension,” International Journal of Multiphase Flow **61**, 37 – 47 (2014).

²⁵W. C. de Jesus, A. M. Roma, M. R. Pivello, M. M. Villar, and A. da Silveira-Neto, “A 3d front-tracking approach for simulation of a two-phase fluid with insoluble surfactant,” Journal of Computational Physics **281**, 403 – 420 (2015).

²⁶P. J. Colucci, F. a. Jaberi, P. Givi, and S. B. Pope, “Filtered density function for large eddy simulation of turbulent reacting flows,” Physics of Fluids **10**, 499 (1998).

²⁷J. M. Vedovoto, A. da Silveira Neto, L. F. F. da Silva, and A. Mura, “Influence of synthetic inlet turbulence on the prediction of low mach number flows,” Computers & Fluids **106**, 135 – 153 (2015).

²⁸T. D. Hanson, “A Hash Table for C Structures,” Accessed in February 09, 2016. (2013).

²⁹J. Ferziger and M. Peric, *Computational Methods for Fluid Dynamics* (Springer, 1996).

³⁰C. Fureby, “Towards the use of Large Eddy Simulation in engineering,” Progress in Aerospace Science **54**, 381–396 (2008).

³¹M. Germano, “Turbulence: the filtering approach,” Journal of Fluid Mechanics **238**, 325–

336 (1992).

³²S. B. Pope, “The Statistical Theory of Turbulent Flames,” Philosophical Transactions of the Royal Society A: Mathematical, Physical and Engineering Sciences **291**, 529–568 (1979).

³³V. Raman, “Hybrid finite-volume/transported PDF simulations of a partially premixed methane-air flame,” Combustion and Flame **136**, 327–350 (2004).

³⁴C. Gardiner, *Stochastic Methods: A Handbook for the Natural and Social Sciences* (Springer, 2009) p. 447.

³⁵F. Barbi, M. R. Pivello, M. M. Villar, R. Serfaty, A. M. Roma, and A. d. Silveira Neto, “Numerical experiments of ascending bubbles for fluid dynamic force calculations,” Journal of the Brazilian Society of Mechanical Sciences and Engineering **40**, 519 (2018).

³⁶B. A. de Freitas Duarte, R. Serfaty, and A. da Silveira Neto, “Influence of the prandtl number on wall-to-fluid thermal transfer rate in a cubic cavity,” Flow, Turbulence and Combustion **103**, 345–367 (2019).

³⁷B. A. d. F. Duarte, R. Serfaty, and A. d. S. Neto, “Direct contact condensation jet in cross-flow using computational fluid dynamics,” Journal of Heat Transfer **141** (2019), 10.1115/1.4042779, 041501.

³⁸M. A. Alves, P. J. Oliveira, and F. T. Pinho, “A convergent and universally bounded interpolation scheme for the treatment of advection,” International Journal for Numerical Methods in Fluids **41**, 47–75 (2003).

³⁹M. M. R. Damasceno, J. G. de Freitas Santos, and J. M. Vedovoto, “Simulation of turbulent reactive flows using a fdf methodology advances in particle density control for normalized variables,” Computers & Fluids **170**, 128 – 140 (2018).

⁴⁰R. S. de Lima, *Desenvolvimento e implementação de malhas adaptativas bloco-estruturadas para computação paralela em mecânica dos fluidos*, Ph.D. thesis, Universidade Federal de Uberlândia (2012).

⁴¹E. Lusk, N. Doss, and A. Skjellum, “A high-performance, portable implementation of the mpi message passing interface standard,” Parallel Computing **22**, 789–828 (1996).

⁴²E. Gabriel, G. E. Fagg, G. Bosilca, T. Angskun, J. J. Dongarra, J. M. Squyres, V. Sahay, P. Kambadur, B. Barrett, A. Lumsdaine, R. H. Castain, D. J. Daniel, R. L. Graham, and T. S. Woodall, “Open MPI: Goals, concept, and design of a next generation MPI implementation,” in *Proceedings, 11th European PVM/MPI Users’ Group Meeting* (Budapest,

Hungary, 2004) pp. 97–104.

⁴³P. Colella and K. Pao, “A projection method for low speed flows,” Journal of Computational Physics **149**, 245–269 (1999).

⁴⁴C. Strozzi, J. Sotton, A. Mura, and M. Bellenoue, “Experimental and numerical study of the influence of temperature heterogeneities on self-ignition process of methane-air mixtures in a rapid compression machine,” Combustion Science and Technology **180**, 1829–1857 (2008).

⁴⁵I. Vincovik, *Dispersion et Mlange Turbulents de Particules Solides et de Gouttelettes par Une Simutatior des Grandes Échelles et Une Modlisation Stochastique Lagrangienne*, Ph.D. thesis, L’Ecole Central de Lyon, Lyon (2005).

⁴⁶Y. Z. Zhang and D. C. Haworth, “A general mass consistency algorithm for hybrid particle/finite-volume pdf methods,” Journal of Computational Physics **194**, 156 – 193 (2004).

⁴⁷H. Möbus, “Comparison of Eulerian and Lagrangian Monte Carlo PDF methods for turbulent diffusion flames,” Combustion and Flame **124**, 519–534 (2001).

⁴⁸V. Sabel’nikov, M. Gorokhovski, and B. N, “The extended iem mixing model in the framework of the composition pdf approach: Applications to diesel spray combustion,” Combustion Theory and Modelling **10**, 155–169 (2006).

⁴⁹M. Cassiani, a. Radicchi, J. Albertson, and U. Giostra, “An efficient algorithm for scalar PDF modelling in incompressible turbulent flow; numerical analysis with evaluation of IEM and IECM micro-mixing models,” Journal of Computational Physics **223**, 519–550 (2007).